ISSN 1809-4430
*www.engenhariaagricola.org.br*

http://dx.doi.org/10.1590/1809-4430-Eng.Agric.v46e20240081/2026

***Scientific Paper***

# Effects of symmetrical spiral anti-blocking and row-sorting device parameters on wheat no-tillage sowing quality

Yunxiang Li[1], Bo Deng[2], Caiyun Lu[2*], Hongwen Li[2], Yuxing Wang[2]

[1] Beijing Institute of Technology, Beijing 100081, China.
[2] College of Engineering, China Agricultural University, Beijing 100083, China.
* Corresponding author: lucaiyun@cau.edu.cn

**How to cite:** Li, Y., Deng, B., Lu, C., Li, H., & Wang, Y. (2026). Effects of symmetrical spiral anti-blocking and row-sorting device parameters on wheat no-tillage sowing quality. *Engenharia Agrícola, 46,* e20250081. http://dx.doi.org/10.1590/1809-4430-Eng.Agric.v46e20250081/2026

## Abstract

This paper analyzes the effects of the parameters of a symmetrical spiral anti-blocking and row-sorting device (SSARD) on the quality of no-tillage wheat sowing. The discrete element method was used to simulate the operating process of the SSARD in the soil bin. The effects of the outer diameter of the symmetrical row-sorting blade, the type of additional stubble-cutting and soil-breaking mechanism (ASSM), the radius of the side baffle notch, the length between the material hopper and the ground, and the width between the opener and the straw baffle on the straw removal rate and the blockage rate were studied. The analysis showed that the straw removal rate of the SSARD improved after optimization, and that the ASSM could cut and chop straw alternately at different rotary velocities. The ASSM could also cut the clods that accumulated on the straw baffle inside with support. The blockage rate was reduced. The response surface method was then used to determine the optimal combination of parameters for the SSARD. The results of a field verification test showed that the straw removal rate of the SSARD could reach 93.35% after optimization, representing an increase of 27.7% compared with a no-till planter without SSARD.

**Keywords**: no-till sowing, anti-blocking, row-sorting of straw, seed belt cleaning, symmetrical spiral.

## Introduction

No (or minimum) tillage sowing is an eco-friendly and sustainable mode of tillage in which straw and stubble from crops on the ground surface are covered without the use of a moldboard plow. This approach falls into the category of conservation agriculture. Unlike traditional modes of tillage, conservation tillage can effectively alleviate soil erosion from wind and water (Uri et al., 1998, 1999), and allows water to be stored in the soil to promote the growth of surface roots (Lampurlanés et al., 2001). The long-term use of conservation tillage can improve crop yields (Gao, 2007). Today, conservation tillage technology has been popularized and applied in more than 70 countries, including the United States and Canada. The area to which global conservation tillage is applied has reached 170 million hectares, accounting for 11% of the total area of cultivated land. In China, research into no/minimum-tillage sowing technologies has been ongoing since the 1950s (State Council, 2020), and by 2025, the implementation area of conservation tillage on black soils in Northeast China had exceeded 100 million mu. During the period of the 14th Five-Year Plan, the cumulative area of black soil

Area Editor: Fábio Lúcio Santos
Received in: 5-7-2024
Accepted in: 11-10-2025



*Edited by*

protected through such practices surpassed 400 million mu-times (Ministry of Agriculture and Rural Affairs, 2022). In recent years, conservation tillage has developed rapidly; it is now widely used, and is becoming one of the fastest growing new technologies in China in terms of relative use rate.

When sowing using a traditional mode of tillage, seeds are delivered by the planter into the soil along a predetermined trajectory, based on the interaction between the soil-contacting components and the soil. In contrast, straw mulching is the main feature of conservation tillage. Unlike the two-factor interaction involving the soil and machine in traditional tillage, there is an interaction between three factors in no/minimum-tillage sowing, involving the soil, machine and straw, which reflects the importance of the straw. When winter wheat is sown using a no-tillage method in the annual double cropping areas of Huang-Huai-Hai in China, the field is covered with a large amount of chopped corn straw. As a result, a no-tillage planter can easily become blocked, causing a severe problem of poor passability for these machines.

In response to this problem of poor passability, researchers are currently focusing on the development of anti-blocking components based on different straw cleaning principles. Liao et al. (2004) described standard anti-blocking technology, in which cutting or separating working components are used to cut or clean the straw or residues at the seeding belt. Baker et al. (2007) and Karayel & Šarauskis (2011) reported that single-disk and double-disk openers were widely used, due to their strong ability to cut and handle straw residues; these are typical cutting anti-blocking components. Lin et al. (2015) designed a spiral notched-disk stubble breaker by selecting an Archimedes spiral as the edge curve for the stubble breaker based on a double-disk stubble breaker, which has a better cutting and anti-blocking effect on soil straw and stubble. McLaughlin et al. (2019) investigated the operational performance of hoe and triple-disk furrow openers in the separating anti-blocking components and compared these with the disk opener. The results showed that the sowing quality of no-till planters installed in two different openers was basically the same. Niu et al. (2019) proposed an anti-blocking idea based on separating and guiding the straw, and designed a clearing wheel based on an Archimedes spiral to guide the straw along the claw. The straw was then thrown out via the rotation of the wheel, thereby alleviating the blockage of the machine. Further research showed that the straw cut by the anti-blocking component could easily be thrown back onto the seeding belt, thus reducing the straw-cleaning effect in the seeding belt and affecting the implantation of seeds and the quality of the seedlings. Hence, cleaning the straw from the seeding belt has become a further problem in no-tillage sowing that needs to be solved urgently, and this is an important research topic.

The various components for cleaning of the seed belt that have been designed to solve this problem in recent years can be divided into two types, based on active and passive operation. Wang et al. (2019) studied the operating mechanism and structural parameters of a star-toothed straw-clearing surface for a concave-disk type mechanism, in which straw was thrown laterally along the tangential direction of a star-toothed concave surface with a relatively high straw removal rate (SRR). Yuan et al. (2021) studied a longitudinal dislocation arrangement for a straw cleaning mechanism, which was designed to separate the straw from the seeding belt, thereby improving the quality of no-tillage corn sowing in drip irrigation areas. Hou et al. (2022) designed an active straw-clearing knife roller with a spiral arrangement on both sides. This knife roller underwent constant rotation, cutting and throwing straw, in order to clean the straw horizontally from the inside of the seeding belt to the outside, which solved the problem of straw ridges.

The analysis presented above shows that the leading indicators affecting the operational performance of no-till planters are the field passability of the machine and the quality of the straw cleaning process in the seeding belt. Although scholars around the globe have carried out a great deal of research on each of these issues individually, few studies have considered these factors simultaneously. In previous work by the current authors (Li et al., 2022), a symmetrical spiral row-sorting mechanism was designed for a straw device; the feasibility of the design principle was proved through preliminary research, and the straw cleaning quality of the seeding belt was relatively improved. However, there was still much room for improvement in terms of field passability, as the machine needs to add and match the most suitable anti-blocking elements. In addition, the performance of the machine was not maximized, since its structure and related parameters had not been optimized.

Since many factors affect the operational performance of the SSARD, it is complicated and expensive to carry out field orthogonal tests by manufacturing corresponding devices with different size parameters. More importantly, it is difficult to clearly elucidate the effects of these factors on the above indicators in macroscopic field tests. However, this is precisely the advantage of the discrete element method (DEM), which is often applied to simulate the operational effect of no/minimum-tillage sowing equipment under conditions with straw mulching on the ground surface, or to design and optimize the structure and parameters of the soil-contacting components based on a theoretical analysis of their operating processes. This method addresses the limitations arising from seasonal changes. In addition, it allows the displacement, velocity, force, and other relevant information to be observed from a microscopic perspective, enabling the mechanism of operation to be understood and providing data support for optimal design.

In this domain, Fang et al. (2016a) simulated and analyzed the motion of straw and soil in the EDEM system, explored the macroscopic and microscopic interactions between the straw, soil and rotary blade, and searched for the optimal working parameters of the rotary blade based on simulation results. Zhao et al. (2020) used the DEM to simulate the strip tillage process with different blades, and analyzed the relationship between the effects of blades with various edge-curve shapes and the disturbance and penetration resistance of the soil. Li et al. (2021) analyzed the effect of the distance between the left and right blades on the SRR using DEM, and optimized the critical parameters of the opposite-placed anti-blocking mechanism. Based on an EDEM simulation, Shi et al. (2019) explored the effect of the working parameters of a minimum-tillage planter on the strip-laying of straw. The order of significance for these parameters was determined, and the accuracy and effectiveness of the EDEM model and discrete element simulation were demonstrated through field tests.

In this paper, the structure and parameters of the SSARD are designed based on the description given above. A discrete element simulation test is carried out in which the outer diameter of the symmetrical row-sorting blade (ODSB), the ASSM, the radius of the side baffle notch (RSBN), the length between the material hopper and the ground (LMHG), and the width between the opener and the straw baffle (WOSB) are considered as the test factors, and the SRR and blockage rate (BR) are used as the test indicators. The optimal parameters are determined by analyzing the mechanism of influence of the interaction between the SSARD, soil and straw, and field tests are conducted to verify the simulation results.

## Material and Methods

### Introduction to the SSARD

The SSARD was installed on the 2BMQF-6/12A no-tillage fertilization planter, and its overall structure is shown in Figure 1.

The high-velocity rotating no-till anti-blocking knife and the ASSM are combined to form a "double-rotated knife". This alternately cuts and chops the straw wrapped around the tillage component at different rotary velocities. Simultaneously, the rotating ASSM and the straw baffle combine to form a "rotated-fixed knife" to cut and chop the clods that accumulate on the straw baffle inside with support in order to improve the field passability of the machine. In addition, as the spiral shaft rotates, the symmetrical row-sorting blades discharge the straw thrown into the materials hopper by the no-till anti-blocking knife to both sides. Under the joint action of the straw baffle and the side baffle, the straw is transported to the non-seeded area on both sides of the seeding belt, thereby achieving row-sorting of the straw and improving the straw-cleaning effect of the seeding belt.

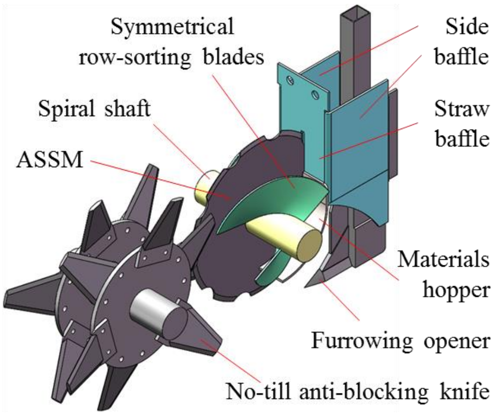


**Figure 1.** Structure of the SSARD.

The operational performance of the SSARD is directly affected by the selection of the critical parameters and their values. It is therefore necessary to design and optimize the critical parameters and their levels for the SSARD.

### Design of the discrete element simulation

### Determination of critical factors and their levels

### ODSB (*D*)

The primary function of the symmetrical row-sorting blades is to row-sort the straw on the seeding belt into the non-seeded area. The main parameters that affect the row-sorting performance are the value of $D$ for the ODSB, the rotary velocity $n$ of the spiral shaft, and the width $W$ of the symmetrical row-sorting blades. The value of $W$ is determined by the agronomic conditions (in this case, no-tillage sowing of wheat in Huang-Huai-Hai's annual double cropping areas), and should be equal to the width of the seeding belt. In this case, the width $W$ of the symmetrical row-sorting blades was designed to be 150 mm (Li et al., 2022b). Since the width remains constant, the gap between the blades gradually increases as $D$ becomes larger.

The value of $D$ for the ODSB directly affects the maximum bearing capacity of the SSARD in terms of conveying straw. The range of values for $D$ given in the literature (Wulantuya et al., 2015 and 2016) is 150–250 mm. In addition, the rotary velocity $n$ of the spiral shaft is determined by the value of $D$. When $n$ is taken as the minimum critical rotary velocity of the motion trajectory of the tip of the symmetrical row-sorting blades as a trochoid, the centrifugal force on the blades is a minimum. In this case, the tip of the symmetrical row-sorting blades spreads the straw to the side and rear at the lowest point, which can achieve the preset operation effect (Li et al., 2022a). The relationship between these quantities is shown in Figure 2.

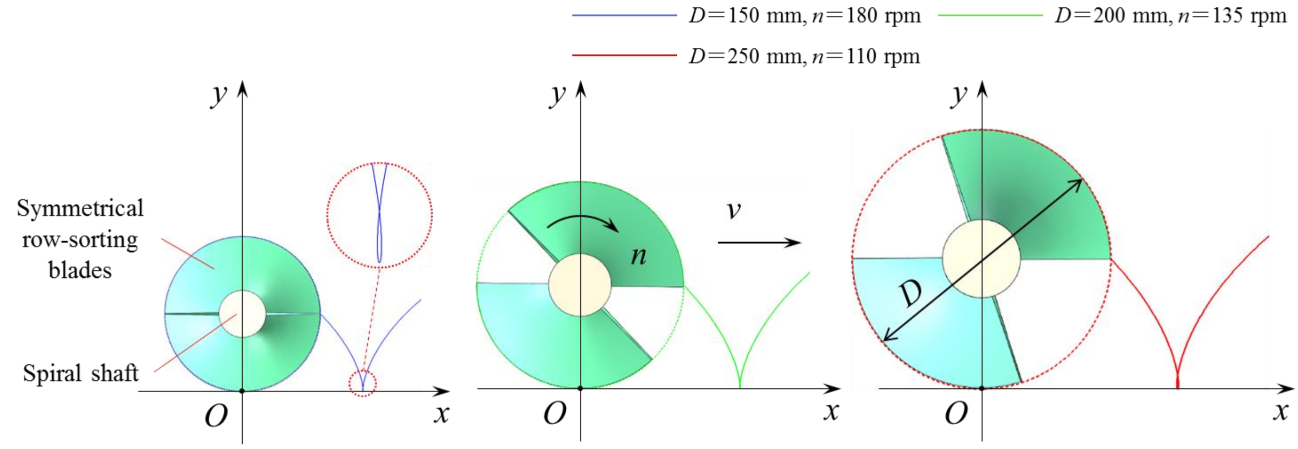


**Figure. 2** Relationship between *D* for the ODSB and the rotary velocity *n* of the spiral shaft.

## ASSM

The addition of a new stubble-cutting and soil-breaking mechanism could improve the broken degree of straw and soil, thus improving the field passability of the machine. Since the anti-blocking performance of the notched disk knife and rotary tillage knife is excellent, in this paper, we consider an additional notched disk knife (Figure 3a), an additional rotary tillage knife (Figure 3b), and a control group without additional structure (Figure 3c) as three different levels for the ASSM. The scientific mechanisms of the different approaches and the corresponding indicators are then tested and analyzed, and the optimal approach is selected.

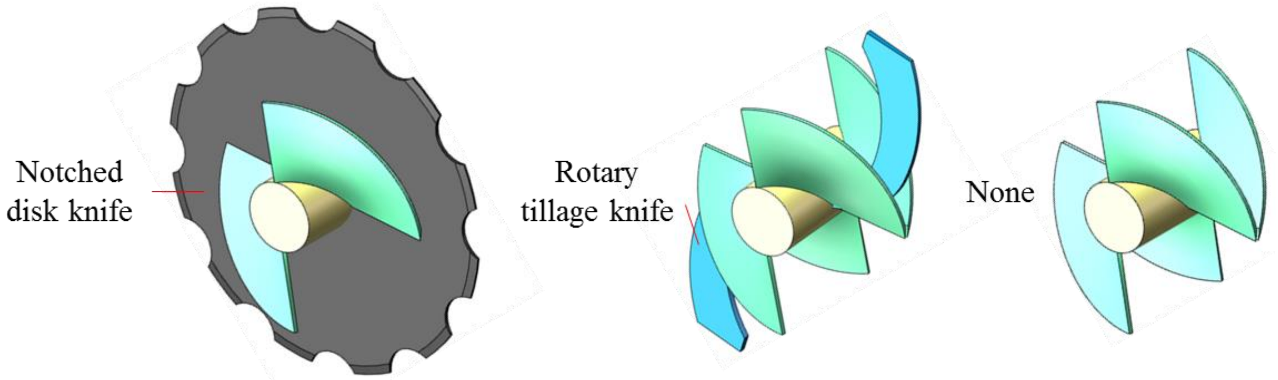


(a) Additional notched disk knife (b) Additional rotary tillage knife (c) Control without additional structure

**Figure. 3** Different types of ASSM for the SSARD.

## RSBN (*Φ*)

The notches in the front part of the side baffle were designed to help to clean the clods resulting from the operation of the opener. However, the shape and size of these notches may affect the field passability and straw-cleaning ability of the SSARD. Three shapes for the notches were designed for the side plate: a linear type (Figure 4a), a convex type (Figure 4b), and a concave type (Figure 4c).

Since the effective discharge area of the concave notch was the largest, the value of *Φ* for the RSBN could be flexibly designed to improve the field passability of the machine without decreasing the SRR. The operational effectiveness of each of the three types of notch was verified by pre-experimentation with discrete element simulations, and the most suitable for the side baffle was determined to be the concave notch. The range for the value of *Φ* for the RSBN was determined as 240–340 mm through the simulation pre-experiment.

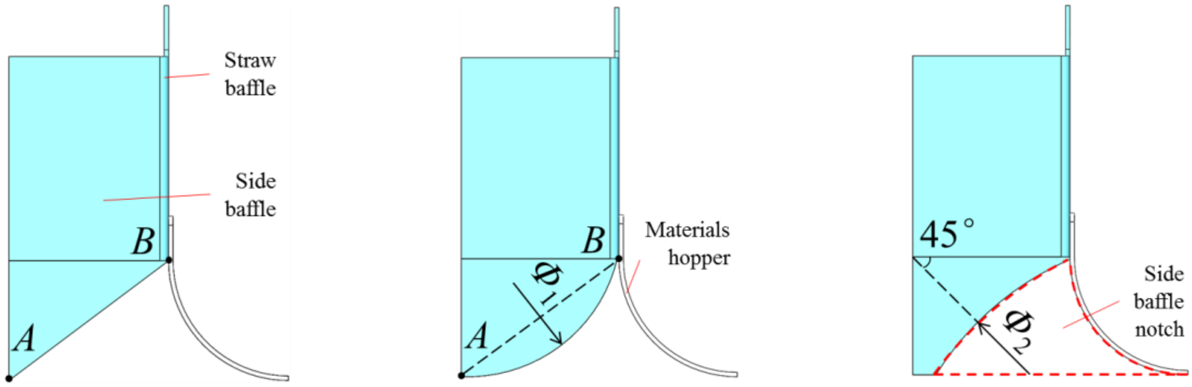


(a) Linear-type notch (b) Convex-type notch (c) Concave-type notch

**Figure. 4** Designs for the side baffle notch.

### LMHG (*h*)

As shown in Figure 5a, the longitudinal spacing between the material hopper and the ground surface needs to be chosen appropriately. The value of *h* for the LMHG should be greater than zero to avoid direct contact between the material hopper and the ground surface, which would cause unnecessary soil disturbance and extra working resistance.

A suitable range of values for *h* of the LMHG was found to be 10–50 mm based on pre-experiments with discrete element simulations, and the actual size was then determined through a formal test.

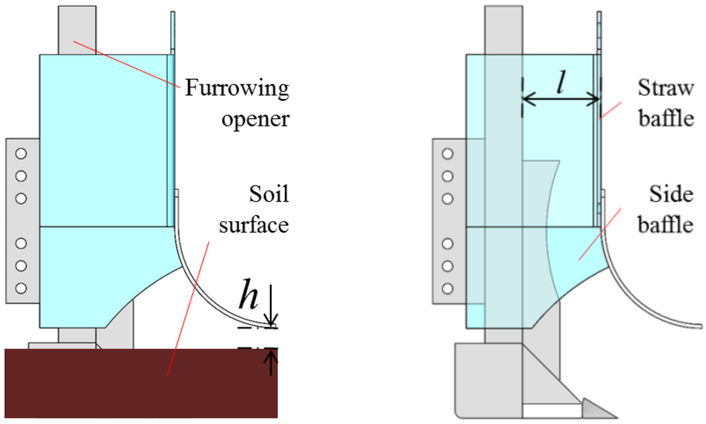


(a) h (b) l

**Figure 5.** *h* for the LMHG and *l* for the WOSB

### WOSB (*l*)

As shown in Figure 5b, the furrowing opener and the straw baffle also require a suitable lateral spacing to ensure regular and effective operation. Ultimately, the range of *l* for the WOSB was determined as 100–200 mm.

### Summary of all factors

As shown in Figure 6, the value of *D* for the ODSB ($X_1$), the ASSM ($X_2$), and the values of $\Phi$ for the RSBN ($X_3$), *h* for the LMHG ($X_4$), and *l* for the WOSB ($X_5$) were selected as the test factors for the discrete element simulation test, and the SRR ($Y_1$) and BR ($Y_2$) were selected as the test indicators. In the analysis presented above, it was determined that the values for $X_1$ (ODSB) were 150, 200, and 250 mm. For $X_2$ (ASSM), three approaches were considered: no additional structure, an additional notched disk knife, and an additional rotary tillage knife. The values for $X_3$ (RSBN) were 240, 290, and 340 mm, whereas the values for $X_4$ (LMHG) were 10, 30, and 50 mm, and the values for $X_5$ (WOSB) were 100, 150, and 200 mm.

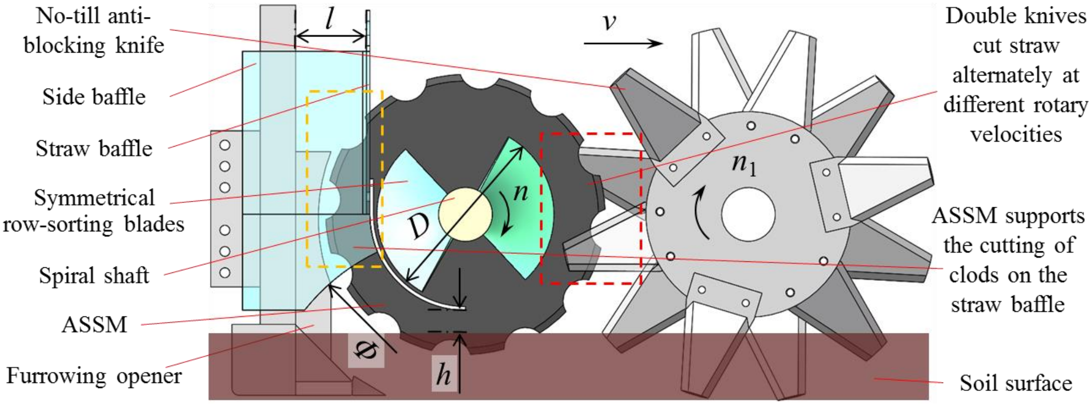


**Figure 6.** Locations of the components considered in the simulations.

As it was difficult to directly compute the optimal values of these factors using existing theoretical equations, the Box–Behnken method from Design Expert 10.0.7 software was used. A quadratic rotation orthogonal combination simulation test was conducted in EDEM software, and the numerical relationships between the test factors and indicators were analyzed via DEM. The parameters and codes considered in these experiments are shown in Table 1.

**Table 1.** Test factors and coding.

| Code | Parameters/approaches | | | | |
|---|---|---|---|---|---|
| | ODSB $X_1$/mm | ASSM $X_2$ | RSBN $X_3$/mm | LMHG $X_4$/mm | WOSB $X_5$/mm |
| −1 | 150 | None | 240 | 10 | 100 |
| 0 | 200 | Notched disk knife | 290 | 30 | 150 |
| 1 | 250 | Rotary tillage knife | 340 | 50 | 200 |

**Establishment of the discrete element simulation model**

Before conducting the EDEM simulation test, a virtual model of the soil bin was first established, with DEM parameters as shown in Table 2 (Wang et al., 2017; Zhao et al., 2021). In order to prevent the number of particles from being too large, which would affect the calculation and simulation efficiency of the workstation, a single spherical particle with a radius of 5 mm was used as a soil particle model (Fang et al., 2016b). In addition, a Hertz–Mindlin (no slip) contact model was applied as the mechanical relationship between all particles.

**Table 2.** DEM parameters.

| Parameter | Value |
|---|---|
| Poisson’s ratio for soil | 0.38 |
| Simulation density for soil particles/(kg/m$^3$) | 1850 |
| Shear modulus of soil/Pa | 1.0×10$^6$ |
| Poisson’s ratio for straw | 0.40 |
| Simulation density for straw particles/(kg/m$^3$) | 240 |
| Shear modulus for straw/Pa | 1.0×10$^6$ |
| Soil–soil recovery coefficient | 0.20 |
| Soil–soil static friction coefficient | 0.40 |
| Soil–soil dynamic friction coefficient | 0.25 |
| Soil–straw recovery coefficient | 0.30 |
| Soil–straw static friction coefficient | 0.30 |
| Soil–straw dynamic friction coefficient | 0.05 |
| Soil–steel recovery coefficient | 0.28 |
| Soil–steel static friction coefficient | 0.50 |
| Soil–steel dynamic friction coefficient | 0.04 |
| Straw–straw recovery coefficient | 0.30 |
| Straw–straw static friction coefficient | 0.30 |
| Straw–straw dynamic friction coefficient | 0.01 |
| Straw–steel recovery coefficient | 0.30 |
| Straw–steel static friction coefficient | 0.30 |
| Straw–steel dynamic friction coefficient | 0.01 |

Since the size parameters used for the straw particle model in the simulation test strongly impact the SRR and BR results, the actual conditions of the straw and its mulching effect on the pre-operation ground surface needed to be simulated as closely as possible. The length and thickness of the straw were uneven and inconsistent after it was chopped and returned to the field, and a normal distribution that closely resembled the actual situation was selected as the size distribution of the straw particles. A straight linear model was chosen for the straw particles. The benchmark model consisted of 22 spherical particles with a radius and spherical center distance of 6 mm, which formed a straw particle model 138 mm in length. Moreover, the length and thickness of the straw model could be adjusted by controlling the average distribution range for the particle radii. Combining with the straw size parameters in Table 3, the mean value of the normal size distribution parameters was set to one and the standard deviation to one. The lower value for the particle size distribution was set to 0.4, and the upper value to 1.6.

After setting the parameters and establishing the virtual soil bin model in the EDEM software, the size of the soil bin was set to 3000×1000×280 mm, and the average mulching thickness of the straw to 47 mm. In addition, considering the actual operating environment and the position of the SSARD in the no-till planter, a plant baffle was built above the virtual soil bin to simulate the actual field conditions as closely as possible. The virtual soil bin is shown in Figure 7.

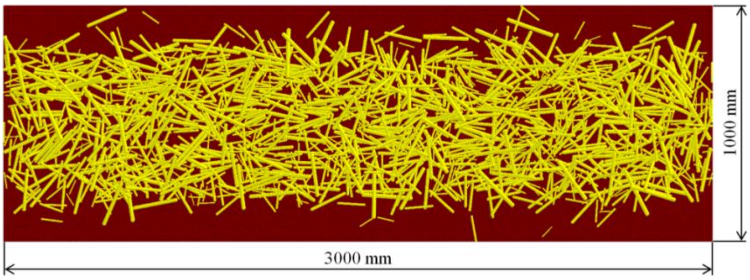


(a) Vertical view

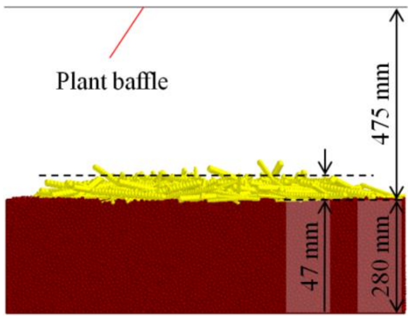


(b) Side view

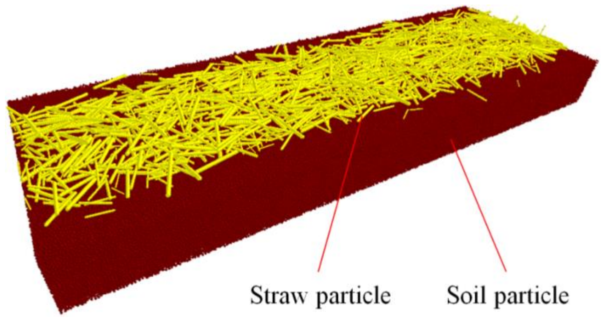


(c) Oblique view

**Figure 7.** Virtual model of the soil bin.

### Test indicators and simulation test methods

Based on the pre-simulation test results, the minimum step size was set to $1.0\times10^{-5}$ s, with a total simulation time of 3.0 s and a target save interval of 0.2 s. A total of 16 sets of temporal nodes were recorded. The mesh size was 9.6 mm, four times the radius of the smallest straw particle. The SSARD operated from the left side of the virtual soil bin and ended at the right side, ultimately leaving the soil bin.

### SRR for the seeding belt in the virtual soil bin

In the domain of no-tillage sowing technology, the SRR of the seeding belt is one of the most important indicators in terms of measuring the effect of no-tillage sowing. The specific value of the SRR is typically calculated by weighing the quality change of straw in the seeding belt before and after operation. In EDEM, as shown in Figure 8, the straw quality change in the virtual soil bin before and after the operation of the SSARD was measured by establishing a straw quality sensor, which was ultimately used to calculate the SRR.

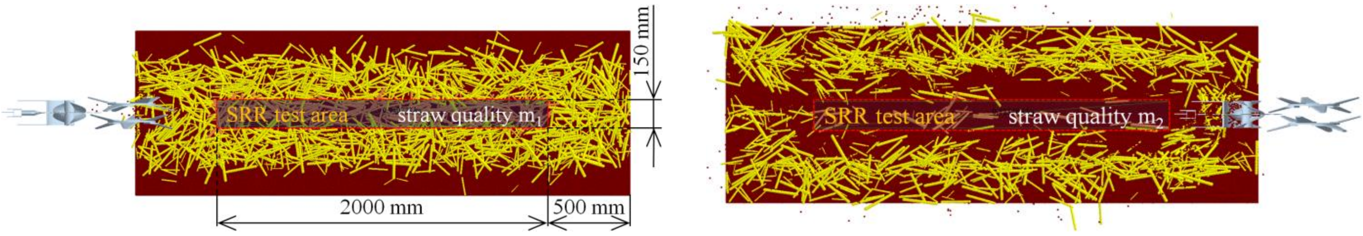


(a) Conditions before SSARD operation

(b) Conditions after SSARD operation

**Figure 8.** SRR test method in EDEM.

Consider the significant impulse of the SSARD just entering the soil bin and the absence of soil and straw particles in front of the device after it leaves the soil bin. This may affect the measurement results of the SRR. A regular working area was set up as the test area, with the center of the soil bin as the midpoint and a length of 2000 mm. The width of the sensor monitoring area was set to 150 mm, equal to the width of the seeding belt. At *t*=0 s, the total mass of straw particles in the test area was denoted as $m_1$, and at *t*=3 s, the total mass of straw particles in the test area was $m_2$. The equation for $\lambda$ is as follows:

$$\lambda = \frac{m_1 - m_2}{m_1} \times 100\% \tag{1}$$

Where:

$\lambda$ is the SRR, %;

$m_1$ is the quality of the straw before operation of the SSARD, kg, and

$m_2$ is the weight of the straw after operation of the SSARD, kg.

**BR in the virtual soil bin**

The industry standard for the passability of machines for no/minimum-tillage sowing, as developed by the Ministry of Agriculture and Rural Affairs, is still qualitatively based, and an observation method is used to judge whether the no-tillage planter is blocked during field operation. There is therefore a need for a quantitative method to analyze the passability of machines in this context.

This paper proposes a method that can be used to quantitatively analyze the passability of a machine in the no-tillage sowing process by DEM. This method requires two soil quality sensors (A and B) and two straw quality sensors (C and D) for quality monitoring. As shown in Figure 9, the length and center of sensors A and C were set to the same as the SRR test area. The top of sensor A was positioned so that it covered the soil particles in the virtual soil bin, while sensor C was set up to cover the centroid of the straw particles. The top of sensor A was in the same plane as the bottom of sensor B, and the top of sensor C was in the same plane as the bottom of sensor D. The lengths of sensors B and D were set equal to the length of the SSARD, and the top plane was slightly higher than the plant baffle. Sensors A and C were fixed, whereas sensors B and D were fixed only in the vertical direction and moved with the SSARD in the horizontal direction. The width of each sensor was 340 mm, equal to the central distance between two adjacent seeding belts. The exact dimensions and positions of all sensors are shown in Figure 9.

Blockage of the machine was mainly due to straw and clods adhering to the soil-contacting components, which were not cleaned in time and kept accumulating, leading to machine failure or system halt. Based on the DEM, the workstation could measure the number of soil and straw particles around the machine in real time and conduct a quantitative analysis of the passability of the machine. When the number of particles around the machine was large, the machine was easily blocked, whereas good passability was observed when the number of particles was small. The straw and soil particles causing blockage of the machine originated from the ground surface. It was therefore more scientific and reasonable to consider the loss of these particles when quantitatively calculating the BR. A higher ratio between the straw and soil particles around the machine and the number of soil and straw particles cut from the ground surface by the no-till anti-blocking knife and spread to the rear makes it easier for the machine to become blocked. Conversely, when the ratio is low, the passability of the machine is good.

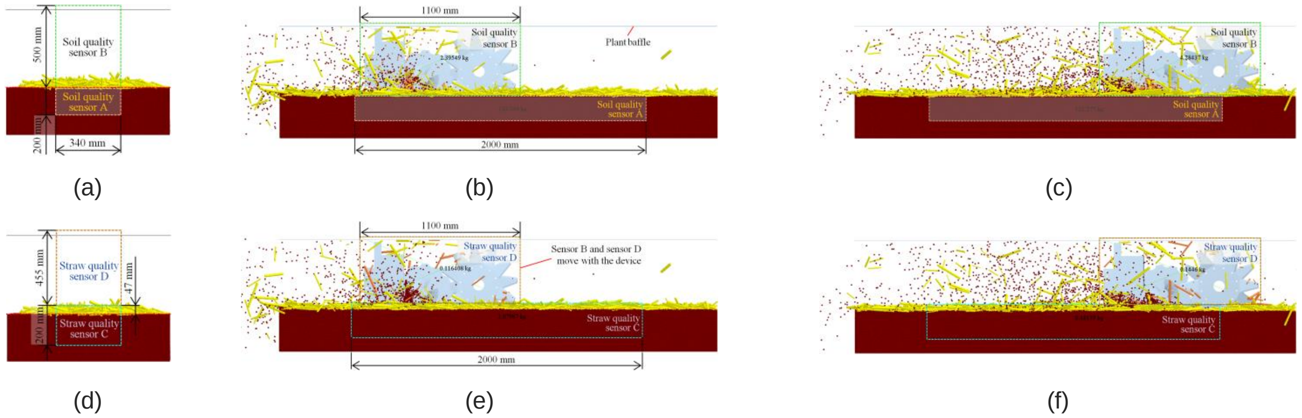


**Figure 9.** Method used to measure of BR and the distribution of sensors in EDEM: (a, d) soil quality sensors A and B, straw quality sensors C and D of the monitoring area side relative position and width, height diagram; (b, e) soil quality sensors A and B, straw quality sensor C and D monitoring area relative position and length diagram; (c, f) relative positions of the soil quality sensor B and straw quality sensor D after installation.

The mathematical model established for calculation of the BR is shown in [eq. (2)]. The denominator of the equation represents the sum of the lost mass $\left(\mathrm{m_A}\big|_{t=3}-\mathrm{m_A}\big|_{t=0}\right)$ of soil particles and the lost mass $\left(\mathrm{m_C}\big|_{t=3}-\mathrm{m_C}\big|_{t=0}\right)$ of straw particles after operation of the machine at the actual position in the virtual soil bin. The numerator represents the maximum total number of straw and soil particles around the machine at $t=i$ s. The use of a ratio in this way can eliminate the influence of the parameter calibration error, and can improve confidence in the test results. The specific values of the BR in each group of simulation tests are calculated using [eq. (2)]:

$$\Delta=\frac{\max\left\{\mu\cdot \mathrm{m_B}\big|_{t=i}+\nu\cdot \mathrm{m_D}\big|_{t=i}\right\}}{\mu\left(\mathrm{m_A}\big|_{t=3}-\mathrm{m_A}\big|_{t=0}\right)+\nu\left(\mathrm{m_C}\big|_{t=3}-\mathrm{m_C}\big|_{t=0}\right)}\times 100\%\,,\quad \left\{i\,\middle|\,0\le i\le 3\right\} \tag{2}$$

Where:

$\Delta$ is the BR, %;

$\mu$ is the soil blockage coefficient;

$\nu$ is the straw blockage coefficient, and

$\mathrm{m_K}$ represents the measurement results for sensor K (where K is A, B, C or D), kg.

## Field test conditions, indicators and methods

### Test conditions

The SSARD was designed and manufactured based on an analysis of the theoretical relationship between the critical factors and the test indicators. On 28th October 2021, a field test was carried out in the machine test base of the Conservation Tillage Research Center of the Ministry of Agriculture and Rural Affairs (No. 152, Luobai Road, Luolong District, Luoyang City, Henan Province. 34°43′20″ N latitude, 112°35′26″ E longitude, air pressure 1008.2 hPa, 137 m above sea level) to verify the actual operation effect of the optimized SSARD.

**Table 3.** Main parameters for field tests.

| Items | Parameters | Values |
|---|---|---|
| Straw in the field | Average length/mm | 138 |
| | Length range/mm | 65–220 |
| | Average diameter /mm | 4.32 |
| | Diameter range /mm | 1–12 |
| | Covering thickness/mm | 47 |
| | SMQ/(kg/m$^2$) | 1.63 |
| | Moisture content/% | 52.65 |
| 0–100 mm soil layer | Firmness /kPa | 665.65 |
| | Moisture content /% | 21.18 |
| | Bulk density /(g/cm$^3$) | 1.37 |
| | Temperature /°C | 17.9 |

The soil at the test site was brown clay, and the temperature at the time of the field test was 20°C (with the temperature on that day varying between 10°C and 20°C), without precipitation. The test conditions are summarized in Table 3. Before the sowing of winter wheat, autumn corn had been planted in June of the same year at the same site, and the corn straw had been chopped and returned to the field.

### Test indicators and methods

#### Passability of the machine

The passability of a machine refers to its ability to exclude crop straw and weeds during no-tillage sowing operations. An industry standard for the passability of machines, entitled *Technical specifications of quality evaluation for no-tillage drilling machinery* (NY/T 1768-2009), was issued by the Ministry of Agriculture and Rural Affairs of the People's Republic of China (2009). For corn straw and stubble fields that have been fallow for two to six months after harvest, the straw mulching quantity is set at 0.7–1.8 kg/m$^2$. Machines are required to make one round trip within a 60 m working distance of the test area at an operating velocity of 5 km/h, as specified in the instruction manual, and the degree of blockage occurring during this process is assessed. A severe blockage occurs if the straw blocks the machine and the operation cannot continue without stopping the machine; however, if a straw blockage occurs and the operation can continue without stopping for cleaning, this is considered a general blockage. A blockage in which straw can automatically flow through the furrowing opener is considered a slight blockage.

#### SRR of the seeding belt

Before the field test started, the five-point sampling method (Ni et al., 2008) was used to measure the straw mass $m_1$ in the pre-operation test area. A 0.25 m$^2$ square metal frame was first applied to a test area that was selected at random. An electronic balance was then used to weigh the quantity of straw mulch in the test area, with the average value recorded as the straw mass $m_1$ before operation.

The formal test was conducted after weighing the straw mass $m_1$. The SSARD was installed on a 2BMQF-6/12A no-till wheat planter, and a test of the straw cleaning effect was conducted at an average operating velocity of 5 km/h in the test area. When the operation was complete, 10 consecutive locations at intervals of 1 m were selected as weighing points for the straw mass $m_2$ in the regular operation area. Ten groups of data were weighed with the electronic balance, and the average value was taken as $m_2$. The specific value of the SRR ($\lambda$) was calculated using [eq. (1)].

## Results and Discussion

### Analysis of the simulation operation process of the SSARD

Observations of the operating process of the 46 groups of the processed test showed that the soil and straw particles largely followed the pre-defined spreading trajectory of the SSARD. This study involved a combination of parameters as follows: $D$ for the ODSB was 250 mm, an additional notched disk knife was used, $\Phi$ for the RSBN was 340 mm, $h$ for the LMHG was 30 mm, and $l$ for the WOSB was 150 mm as an example (Test No. 16). The simulation process is illustrated in Figure 10.

The interaction between the machine, straw, and soil means that the soil and straw particles mainly appear on the left side of the SSARD model during the operation of the SSARD. In contrast, the number of particles floating in the air on the right side is small. When the SSARD spreads the soil and straw particles backwards, they acquire a high velocity at the moment of contact with the machine, and most of these are shown in red. The particles then move backwards and upwards, continue backwards and downwards after hitting the plant baffle, and finally fall into the soil bin on the left side of the machine. The color representing the velocity gradually changes from green to blue. The overall trend in the simulation results is fairly consistent with the actual process in the field.

To explore the interaction between the machine and the straw, straw particles are evenly laid on the right side of the soil bin surface before the SSARD operates. After the operation of this machine, a clean strip is formed on the left side of the SSARD, corresponding to the position of the seeding belt. Only a small amount of straw particles remain on the seeding belt, and most of the straw is discharged to both sides of the SSARD, resulting from the movement of the SSARD. As the spiral shaft rotates, the symmetrical row-sorting blades convey the straw particles, which are spread backwards by the no-till anti-blocking knife, from the material hopper to both sides of the SSARD, thus preventing the straw from falling into the seeding belt.

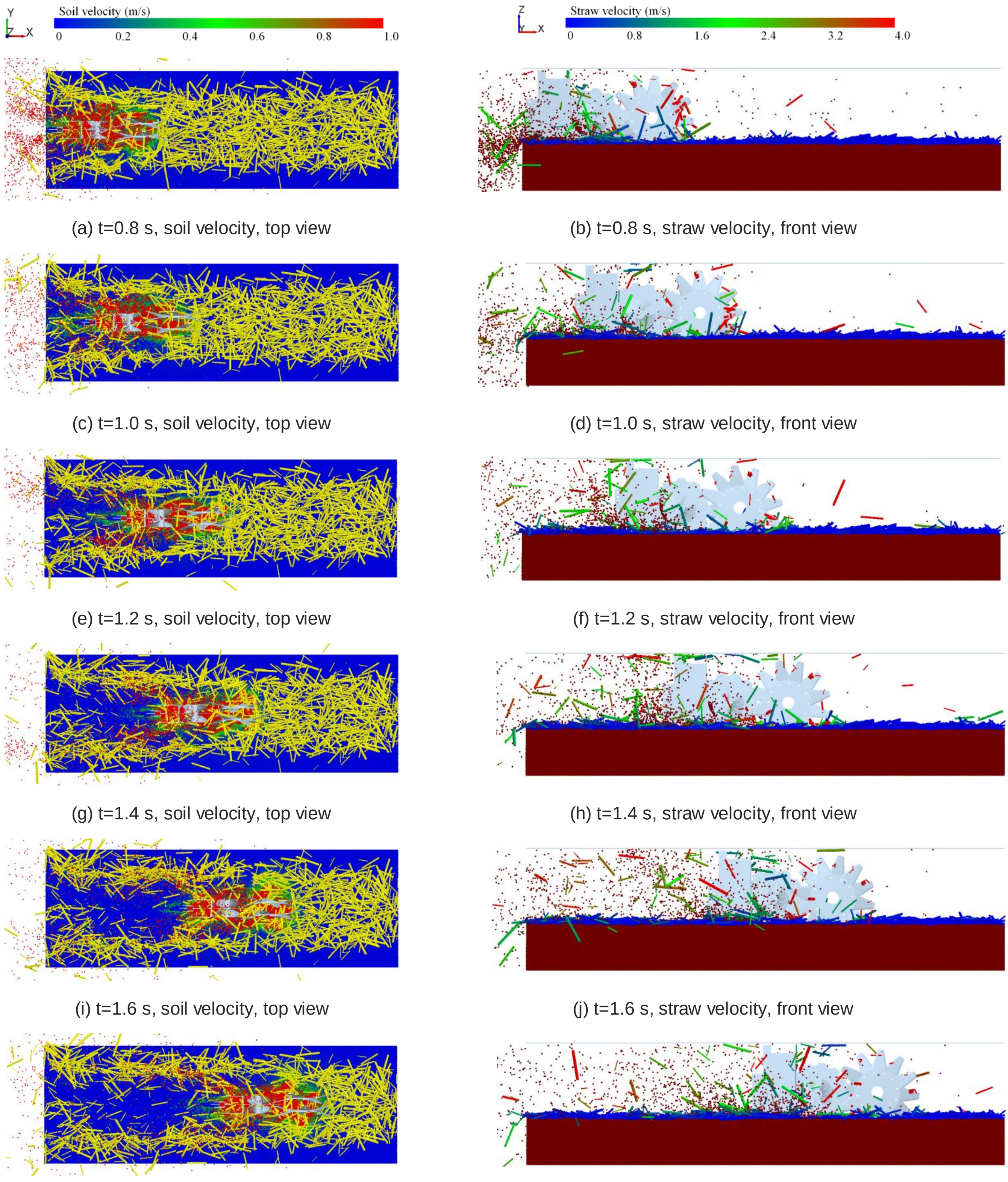


(a) t=0.8 s, soil velocity, top view

(b) t=0.8 s, straw velocity, front view

(c) t=1.0 s, soil velocity, top view

(d) t=1.0 s, straw velocity, front view

(e) t=1.2 s, soil velocity, top view

(f) t=1.2 s, straw velocity, front view

(g) t=1.4 s, soil velocity, top view

(h) t=1.4 s, straw velocity, front view

(i) t=1.6 s, soil velocity, top view

(j) t=1.6 s, straw velocity, front view

(k) t=1.8 s, soil velocity, top view

(l) t=1.8 s, straw velocity, front view

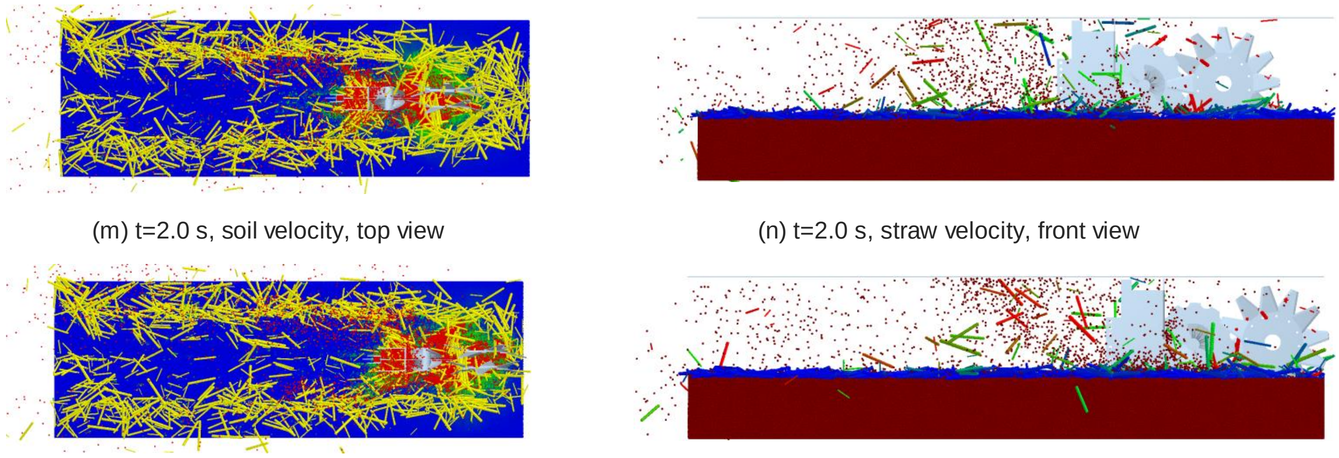

(m) t=2.0 s, soil velocity, top view

(n) t=2.0 s, straw velocity, front view

(o) t=2.2 s, soil velocity, top view

(p) t=2.2 s, straw velocity, front view

**Figure 10.** Visualization of results from the discrete element simulation test.

The results for the interaction between the machine and the soil show that the two soil-contacting components (i.e., the no-till anti-blocking knife and the additional notched disk knife) are in contact with the soil particles in turn during the operation, and the soil particles around them are all shown in red. Moreover, in the middle of the virtual soil bin and the plant baffle, soil particles around the SSARD are the most, and on the rear of the machine operation are the second most. This effect is caused by the no-till anti-blocking knife cutting and spreading the soil particles backwards. Due to the small internal space within the SSARD, the soil particles can easily accumulate and adhere, and it is difficult for them to pass through the machine. The soil particles passing through the SSARD are spread behind it, forming dust that is generated during the field operation of the machine.

## Simulation test results and overall analysis

The factors, levels, and results of the simulation tests are shown in Table 4. In general, the ANOVA (Table 5) shows that variations in the parameters for the ODSB ($X_1$), RSBN ($X_3$), LMHG ($X_4$), and WOSB ($X_5$) significantly affect the SRR ($Y_1$) ($P$<0.01). Moreover, variations in the parameters of ASSM ($X_2$), RSBN ($X_3$), LMHG ($X_4$), and WOSB ($X_5$) significantly affect the BR ($Y_2$) ($P$<0.01). Finally, the factors $X_1X_3$ ($P$=0.02) and $X_1X_4$ ($P$=0.015) have a significant interaction effect on $Y_1$, whereas the factors $X_2X_3$ ($P$<0.01) and $X_3X_4$ ($P$<0.01) have a highly significant interaction effect on $Y_2$.

**Table 4.** Test combinations and results

| Test no. | Factors | | | | | Response values | |
|---|---|---|---|---|---|---|---|
| | $X_1$ (mm) | $X_2$ | $X_3$ (mm) | $X_4$ (mm) | $X_5$ (mm) | $Y_1$ (%) | $Y_2$ (%) |
| 1 | −1 | −1 | 0 | 0 | 0 | 73.29 | 18.95 |
| 2 | 1 | −1 | 0 | 0 | 0 | 89.49 | 16.76 |
| 3 | −1 | 1 | 0 | 0 | 0 | 71.58 | 14.71 |
| 4 | 1 | 1 | 0 | 0 | 0 | 88.54 | 13.83 |
| 5 | 0 | 0 | −1 | −1 | 0 | 88.72 | 13.55 |
| 6 | 0 | 0 | 1 | −1 | 0 | 83.2 | 17.43 |
| 7 | 0 | 0 | −1 | 1 | 0 | 78.34 | 14.28 |
| 8 | 0 | 0 | 1 | 1 | 0 | 70.2 | 11.15 |
| 9 | 0 | −1 | 0 | 0 | −1 | 77.1 | 16.28 |
| 10 | 0 | 1 | 0 | 0 | −1 | 73.7 | 13.88 |
| 11 | 0 | −1 | 0 | 0 | 1 | 75.28 | 15.24 |
| 12 | 0 | 1 | 0 | 0 | 1 | 70.34 | 11.35 |
| 13 | −1 | 0 | −1 | 0 | 0 | 78.94 | 13.39 |
| 14 | 1 | 0 | −1 | 0 | 0 | 91.04 | 12.26 |
| 15 | −1 | 0 | 1 | 0 | 0 | 62.78 | 11.18 |
| 16 | 1 | 0 | 1 | 0 | 0 | 89.83 | 10.97 |
| 17 | 0 | 0 | 0 | −1 | −1 | 84.42 | 14.73 |
| 18 | 0 | 0 | 0 | 1 | −1 | 78.06 | 13.56 |
| 19 | 0 | 0 | 0 | −1 | 1 | 82.91 | 10.7 |
| 20 | 0 | 0 | 0 | 1 | 1 | 72.28 | 8.68 |
| 21 | 0 | −1 | −1 | 0 | 0 | 79.5 | 22.9 |
| 22 | 0 | 1 | −1 | 0 | 0 | 79.47 | 11.48 |
| 23 | 0 | −1 | 1 | 0 | 0 | 78.67 | 14.87 |
| 24 | 0 | 1 | 1 | 0 | 0 | 76.86 | 12.74 |
| 25 | −1 | 0 | 0 | −1 | 0 | 71.91 | 13.36 |
| 26 | 1 | 0 | 0 | −1 | 0 | 92.71 | 12.43 |
| 27 | −1 | 0 | 0 | 1 | 0 | 75.59 | 12.51 |
| 28 | 1 | 0 | 0 | 1 | 0 | 80.64 | 12.38 |
| 29 | 0 | 0 | −1 | 0 | −1 | 86.34 | 13.78 |
| 30 | 0 | 0 | 1 | 0 | −1 | 79.44 | 10.58 |
| 31 | 0 | 0 | −1 | 0 | 1 | 82.93 | 12.62 |
| 32 | 0 | 0 | 1 | 0 | 1 | 63.87 | 8.42 |
| 33 | −1 | 0 | 0 | 0 | −1 | 71.02 | 12.62 |
| 34 | 1 | 0 | 0 | 0 | −1 | 85.43 | 13.05 |
| 35 | −1 | 0 | 0 | 0 | 1 | 69.62 | 11.21 |
| 36 | 1 | 0 | 0 | 0 | 1 | 79.53 | 11.25 |
| 37 | 0 | −1 | 0 | −1 | 0 | 86.34 | 19.63 |
| 38 | 0 | 1 | 0 | −1 | 0 | 83.41 | 15.51 |
| 39 | 0 | −1 | 0 | 1 | 0 | 79.27 | 16.67 |
| 40 | 0 | 1 | 0 | 1 | 0 | 77.93 | 14.44 |
| 41 | 0 | 0 | 0 | 0 | 0 | 70.19 | 12.59 |
| 42 | 0 | 0 | 0 | 0 | 0 | 68.83 | 13.41 |
| 43 | 0 | 0 | 0 | 0 | 0 | 75.94 | 14.13 |
| 44 | 0 | 0 | 0 | 0 | 0 | 73.78 | 11.81 |
| 45 | 0 | 0 | 0 | 0 | 0 | 67.53 | 13.2 |
| 46 | 0 | 0 | 0 | 0 | 0 | 68.65 | 9.98 |

**Establishment of regression model**

The test indicators in Table 4 were used in a regression analysis with Design Expert software, and regression models for $Y_1$ and $Y_2$ on $X_1$, $X_2$, $X_3$, $X_4$, and $X_5$ were established as shown in eqs (3) and (4).

$$Y_1 = 71.86 + 7.65X_1 - 1.07X_2 - 3.78X_3 - 3.83X_4 - 2.42X_5 + 3.74X_1X_3 - 3.94X_1X_4 - 3.04X_3X_5 + 4.35{X_1}^2 + 3.42{X_2}^2 + 4.2{X_3}^2 + 5.52{X_4}^2 \tag{3}$$

$$Y_2 = 12.5 - 0.31X_1 - 2.09X_2 - 1.06X_3 - 0.85X_4 - 1.19X_5 + 2.32X_2X_3 + 0.47X_2X_4 - 0.37X_2X_5 - 1.75X_3X_4 + 3.16{X_2}^2 + 0.8{X_4}^2 - 1.12{X_5}^2 \tag{4}$$

The validity of the regression models was confirmed. The results in Table 5 indicate that the regression models for the test indicators $Y_1$ and $Y_2$ were both highly significant ($P$<0.01). The $P$ value for $Y_1$'s lack of fit was 0.6648, the $P$ value for $Y_2$'s lack of fit was 0.7855, and both tests of the lack of fit were insignificant ($P$>0.1). The values of the coefficient of determination $R^2$ for the regression equation were 0.8727 for $Y_1$ and 0.8508 for $Y_2$; these values are both greater than 85%, and the regression model is therefore valid.

**Table 5.** Results of an ANOVA for two-factor interactive regression equation.

| Source | $Y_1$ (%) | | | | $Y_2$ (%) | | | |
|---|---|---|---|---|---|---|---|---|
| | Sum of squares | Free-dom | $F$ value | $P$ Value | Sum of squares | Free-dom | $F$ value | $P$ Value |
| Model | 2133.22 | 12 | 18.86 | <0.0001** | 288.26 | 12 | 15.69 | <0.0001** |
| $X_1$ | 937.58 | 1 | 99.45 | <0.0001** | 1.56 | 1 | 1.02 | 0.3198 |
| $X_2$ | 18.30 | 1 | 1.94 | 0.1729 | 69.56 | 1 | 45.42 | <0.0001** |
| $X_3$ | 228.24 | 1 | 24.21 | <0.0001** | 17.89 | 1 | 11.68 | 0.0017** |
| $X_4$ | 234.93 | 1 | 24.92 | <0.0001** | 11.68 | 1 | 7.63 | 0.0093** |
| $X_5$ | 93.85 | 1 | 9.95 | 0.0034** | 22.59 | 1 | 14.75 | 0.0005** |
| $X_1X_3$ | 55.88 | 1 | 5.93 | 0.0205* | / | | | |
| $X_1X_4$ | 62.02 | 1 | 6.58 | 0.0151* | / | | | |
| $X_2X_3$ | / | | | | 21.58 | 1 | 14.09 | 0.0007** |
| $X_2X_4$ | / | | | | 0.89 | 1 | 0.58 | 0.4505 |
| $X_2X_5$ | / | | | | 0.56 | 1 | 0.36 | 0.5513 |
| $X_3X_4$ | / | | | | 12.29 | 1 | 8.02 | 0.0078** |
| $X_3X_5$ | 36.97 | 1 | 3.92 | 0.0561 | / | | | |
| $X_1^2$ | 178.37 | 1 | 18.92 | 0.0001** | / | | | |
| $X_2^2$ | 110.19 | 1 | 11.69 | 0.0017** | 98.49 | 1 | 64.31 | <0.0001** |
| $X_3^2$ | 166.21 | 1 | 17.63 | 0.0002** | / | | | |
| $X_4^2$ | 286.80 | 1 | 30.42 | <0.0001** | 6.39 | 1 | 4.18 | 0.0491* |
| $X_5^2$ | / | | | | 12.34 | 1 | 8.05 | 0.0077** |
| Residual | 311.12 | 33 | | | 50.54 | 33 | | |
| Lack of fit | 256.26 | 28 | 0.83 | 0.6648 | 39.73 | 28 | 0.66 | 0.7855 |
| Pure error | 54.87 | 5 | | | 10.81 | 5 | | |
| Cor total | 2444.34 | 45 | | | 338.80 | 45 | | |

Note: ** means highly significant (P<0.01), * means significant (0.01<P<0.05).

Table 5 shows the results of a variance and significance analysis of the regression model. For the test indicator $Y_1$, the factors $X_1$, $X_3$, $X_4$, $X_5$, $X_1^2$, $X_2^2$, $X_3^2$, and $X_4^2$ have highly significant effects, while factors $X_1X_3$ and $X_1X_4$ have significant effects. The order of significance for the five factors influencing $Y_1$ is $X_1 > X_4 > X_3 > X_5 > X_2$. For the test indicator $Y_2$, factors $X_2$, $X_3$, $X_4$, $X_5$, $X_2X_3$, $X_3X_4$, $X_2^2$, and $X_5^2$ have highly significant effects, and factor $X_4^2$ has a significant effect. The order of significance for the five factors influencing $Y_2$ is $X_2 > X_5 > X_3 > X_4 > X_1$. The other items of the regression model are insignificant.

## Influence of changes to a single factor on the test indicators

Using eqs (3) and (4), each factor was considered at different levels, with the remaining factors fixed at a medium level, and the direct impact of the change in its value on the test indicator was calculated. The results are shown in Figure 11. In this section, each factor is analyzed separately to explore the mechanism of influence between the different factors and indicators.

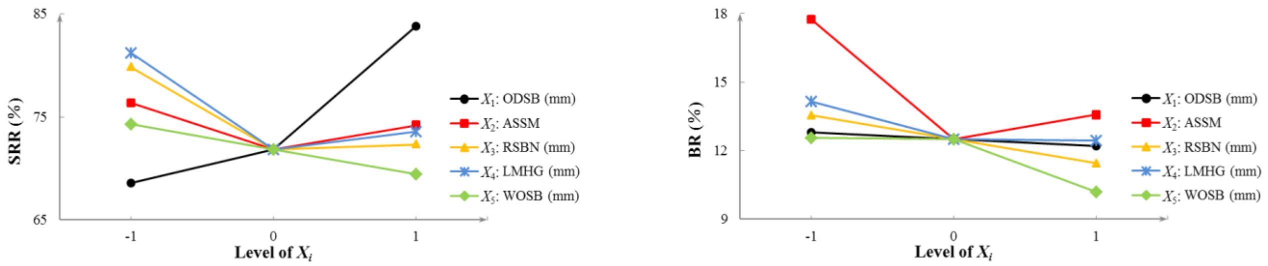


(*a*) Influence of a change in factor values on $Y_1$ (*b*) Influence of a change in factor values on $Y_2$

**Figure 11.** Influence of a change to a single factor on the test indicators.

### ODSB ($X_1$)

As shown in Figure 11a, with an increase in the parameter for the ODSB ($X_1$), the SRR ($Y_1$) of the seeding belt also increases. In a physical sense, the material bearing capacity of the SSARD increases when $X_1$ is increased. Since the rotary velocity of the no-till anti-blocking knife was constant, the amount of straw spread by the knife into the SSARD was also constant within the same period. During the same operation cycle, the ODSB increased, and the rotary velocity of the spiral shaft decreased; this improved the operational stability of row-sorting of the straw while maintaining the same conveying efficiency. The straw was less likely to wrap around the spiral shaft or accumulate in the material hopper, thus reducing the amount of straw that fell into the seeding belt. Ultimately, the SRR $Y_1$ was improved, a finding that aligns with that of our previous study (Li et al., 2022a).

For the BR ($Y_2$), increasing the size of $X_1$ for the symmetrical row-sorting blades improved the soil-conveying efficiency of the SSARD, and improved the field passability of the machine to a certain extent. However, when $X_1$ was increased, the volume of the symmetrical row-sorting blades also became larger, which led to a smaller size of the internal space of the SSARD and increased the possibility of the SSARD becoming blocked. Ultimately, these two effects offset each other, and no significant relationship was found. In addition, when $X_1$ was increased, the BR ($Y_2$) decreased slightly, probably due to the higher conveying efficiency being more dominant than the smaller space.

### ASSM ($X_2$)

When there was no additional structure, it was found that the inside of the straw baffle and side baffle surrounding and protecting the furrowing opener tended to accumulate clods easily, resulting in blockage (Figure 12a). In addition, when the no-till anti-blocking knife was in continuous operation, its blades tended to cause straw and weeds to become wound up in the soil-contacting area (Figure 12b), causing blockage between the groups of anti-blocking knives and affecting the quality of the operation.

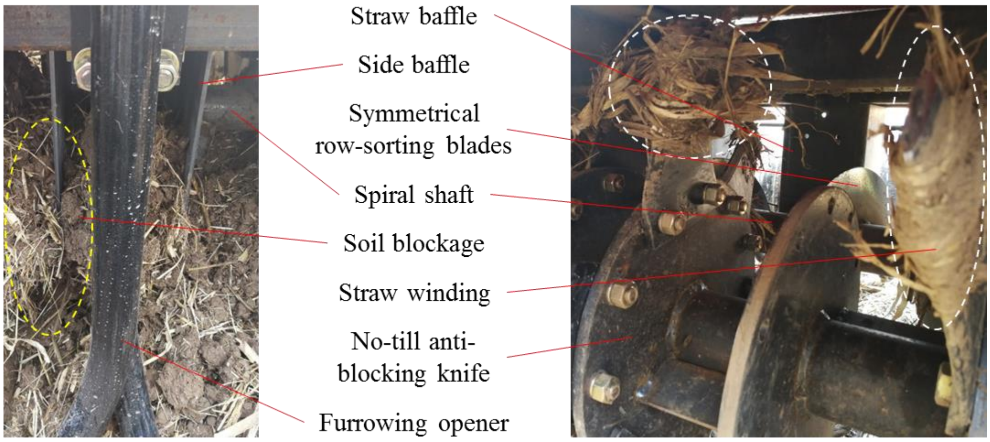


(a) Accumulation of clods in straw baffles resulting in blockage

(b) No-till anti-blocking knife wound with straw and weeds

**Figure 12.** Photographs showing blocking of the SSARD in the field test

Installing the ASSM ($X_2$) reduced the BR ($Y_2$) of the machine for the following reasons. (i) The spiral shaft and the no-till anti-blocking knife shaft rotated in the same direction with different velocities, and the ASSM cut and chopped straw alternately at different rotary velocities with the no-till anti-blocking knife at the space intersection position, which increased the degree of chopping of the clods and straw by the machines (Liu et al., 2020, 2021) and improved the passability of the machine. (ii) In regard to the problem of soil accumulation on the inside of the straw baffle and side baffle, since the straw baffle is fixed and the ASSM rotates clockwise, a new "rotated-fixed knife" combination can be formed on its space-contacting surface. This operates on a supporting cutting principle, and can cut and chop hardened clods (Lu et al., 2013a,b). In this case, it was possible to break the clods that have accumulated on the inside of the straw baffle in time to reduce the blockage in the position shown in Figure 6.

We also note that the additional notched disk knife had a lower BR than the additional rotary tillage knife. The main reason for this was that the notched disk knife was a continuous-disk type, and was always in the working condition as the spiral shaft rotated. With only two sets of rotary blades set on the spiral shaft, it intermittently cut and chopped straw and soil mainly by increasing the impulse. The continuous and uniform cutting effect of the notched disk knife was therefore superior to that of the rotary tillage knife.

Variation in $X_2$ had no significant effect on the SRR ($Y_1$). However, when no additional structure was used, the machine could achieve a higher SRR than when a notched disk knife or rotary tillage knife were used. This was because when the ASSM cut and chopped straw alternately at different rotary velocities with the no-till anti-blocking knife, a small portion of the straw became wrapped around the ASSM, and it was possible for this straw to fall through the gap of the straw baffle into the seeding belt, thus affecting the test results for the SRR. Moreover, in the same cycle, the notched disk knife operated for longer than the rotary tillage knife, which increased the possibility of straw falling onto the seeding belt.

**RSBN ($X_3$)**

The main reason for soil blockage on the inside of the straw baffle and the side baffle was that the furrowing opener spread the broken clods to the rear during the trenching operation, giving rise to a "clod wave" phenomenon (Figure 13) under the action of the machine moving forward. These clods first hit the straw baffle in front, and then flowed to the baffles on both sides. Due to the small distance between adjacent side baffles, the space for movement of the clods was small, making it difficult for them to be discharged in time and causing soil blockage in the actual test.

Increasing the RSBN parameter ($X_3$) would increase the space on both sides of the opener, meaning that within the same amount of time, more clods could be discharged at the notch of the side baffle, thus reducing the BR ($Y_2$) of the machine. A change in $X_3$ had a significant impact on the BR ($Y_2$), indicating that when $X_3$ was 290 mm in the middle level, the passability of the machine had not reached a maximum. There were still some pieces of soil thrown by the opener that had yet to be discharged from the notch of the straw baffle in time, and these could adhere to the inside of the straw baffle and side baffle.

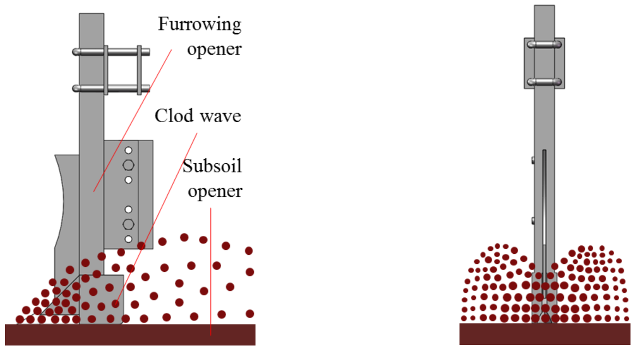


(a) Side view of soil broken by the furrowing opener

(b) Front view of soil broken by the furrowing opener

**Figure 13.** Diagrams showing the "clod wave" phenomenon.

As the value of the RSBN parameter ($X_3$) increased, the SRR ($Y_1$) first decreased and then slightly increased. When $X_3$ was increased from 240 to 290 mm, the possibility of straw falling into the seeding belt from the notch position of the side baffle increased with the notch area, and the SRR ($Y_1$) showed a decreasing trend. However, the soil thrown up by the furrowing opener moved outward from the notch of the side baffle, generating an outward flowing force. Although this prevented the straw from outside falling onto the seeding belt, some straw that remained on the seeding belt was discharged from the notch with the "clod wave". When $X_3$ was set to a medium value of 290 mm, some straw and soil were not discharged in time; when it was increased to 340 mm, the number of soil and straw particles discharged increased slightly, and the SRR ($Y_1$) also increased slightly.

**LMHG ($X_4$)**

As there was a gap between the bottom of the materials hopper and the ground surface, a small portion of the straw in contact with the bottom of the no-till anti-blocking knife could be subjected to a cutting force in the horizontal direction during the process in which straw was spread backwards by the no-till anti-blocking knife. This part of the straw could pass through the gap and fall onto the seeding belt. However, decreasing the value of the LMHG parameter ($X_4$) could reduce the probability of the straw passing through this gap (Li et al., 2022a). The highest SRR ($Y_1$) was therefore achieved when $X_4$ had the minimum value of 10 mm.

The value of $X_4$ was negatively correlated with the BR ($Y_2$). As shown in Figure 12, the straw wrapped around the no-till anti-blocking knife, while the clods accumulated on the inside of the straw baffle and the side baffle, and blockage of the machine occurred mainly at these two locations. Due to the added notch design for the straw baffle, blocking was more difficult in the gap between the material hopper and the ground surface than in the locations described above; for this reason, the factor $X_4$ was much less significant than $X_2$.

**WOSB ($X_5$)**

The value of the SRR ($Y_1$) was negatively correlated with that of the WOSB parameter ($X_5$). As the space between the opener and the straw baffle was increased, the time required for the straw to be thrown to the corresponding position of the opener increased, and the probability of it falling onto the seeding belt also increased slightly (Yuan et al., 2021). However, since the symmetrical row-sorting blades obliquely thrust the straw to both sides of the seeding belt, most of the straw was not subjected to the force in the opposite direction during its movement. Variation in $X_5$ therefore had little effect on the straw falling back onto the seeding belt.

For the BR ($Y_2$), variation in $X_5$ significantly affected the value of $Y_2$, and $Y_2$ was negatively correlated with $X_5$. This was because clods accumulated inside the straw baffle and gradually caused a blockage at the front of the opener. As the WOSB parameter was increased, the space surrounding and protecting the opener between the straw baffle and the side baffle increased. This increased the internal clearance of the SSARD, which allowed for a larger number of clods to be accommodated in the same amount of time, ultimately improving the passability of the machine.

**Influence of interaction factors on test indicators**

**3SRR ($Y_1$)**

From Table 5, it can be seen that $X_1X_3$ and $X_1X_4$ have an interactive impact on $Y_1$, and their response surfaces are shown in Figure 14. To explore the interaction factor $X_1X_3$, we set $X_2$ as the rotary tillage knife, $X_4$ as 30 mm, and $X_5$ as 150 mm. When the level of $X_1$ was unchanged, $Y_1$ showed a trend of first decreasing and then increasing with an increase in $X_3$. When $X_3$ is in the range 240–340 mm, the possibility of straw falling through the notch of the side baffle into the seeding belt increases as the notch becomes larger. However, when $X_3$ is increased to a certain level, some straw will be discharged from the notch with the "clod wave", and $Y_1$ will slightly rebound. In addition, when $X_3$ is constant, $Y_1$ basically increases with $X_1$ and is positively correlated. When $X_1$ is in the range 150–250 mm, the material bearing capacity of the SSARD increases with an increase in $X_1$, the straw conveying efficiency increases, and the SRR will also be effectively improved.

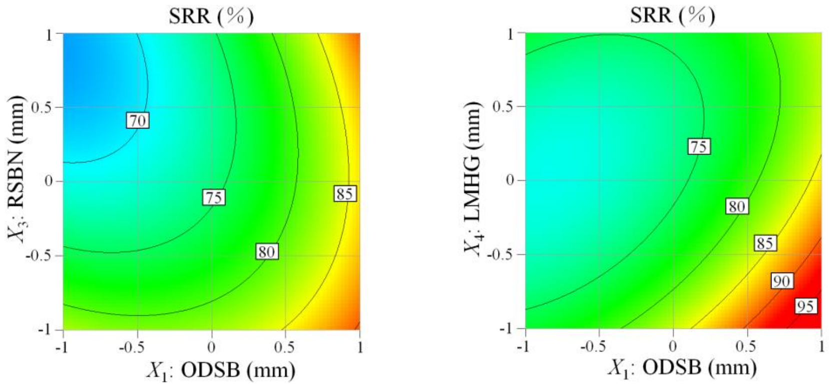


(*a*) $Y_1$=*f* ($X_1$, 1, $X_3$, 0, 0) (*b*) $Y_1$=*f* ($X_1$, 1, 0, $X_4$, 0)

**Figure 14.** Influence of interaction factors on test indicator $Y_1$.

To explore the interaction factor $X_1X_4$, we first fixed factor $X_1$, and set $X_2$ as the rotary tillage knife, $X_3$ as 290 mm, and $X_5$ as 150 mm. When $X_4$ is in the range 10–50 mm and $X_1$ is in the range of 150–212 mm, $Y_1$ shows a trend of first decreasing and then slightly increasing with an increase in $X_4$, which may be due to disturbance to the trajectory of the straw from soil flow. In addition, when $X_1$ is in the range 212–250 mm, $Y_1$ decreases with an increase in $X_4$ and is negatively correlated. The smaller the gap between the material hopper and the ground surface, the smaller the amount of straw that can pass directly through the bottom of the straw baffle during the machine's advance, which increases the SRR.

**BR ($Y_2$)**

From Figure 15, it can be seen that $X_2X_3$ and $X_3X_4$ also have an interactive impact on $Y_2$. To explore the interaction factor $X_2X_3$, we set $X_1$ as 250 mm, $X_4$ as 50 mm, and $X_5$ as 200 mm. When $X_2$ is constant, $Y_2$ decreases with an increase in $X_3$ and is negatively correlated. When $X_3$ is in the range 240–340 mm, an increase in RSBN causes better fluidity of the soil broken by the opener discharged from the notch, and improves the passability of the machine. In addition, when the level of $X_3$ is unchanged, the ASSM $X_2$ reduces $Y_2$. It can also be seen that the notched disk knife has good operating continuity and better anti-blocking performance than the rotary tillage knife.

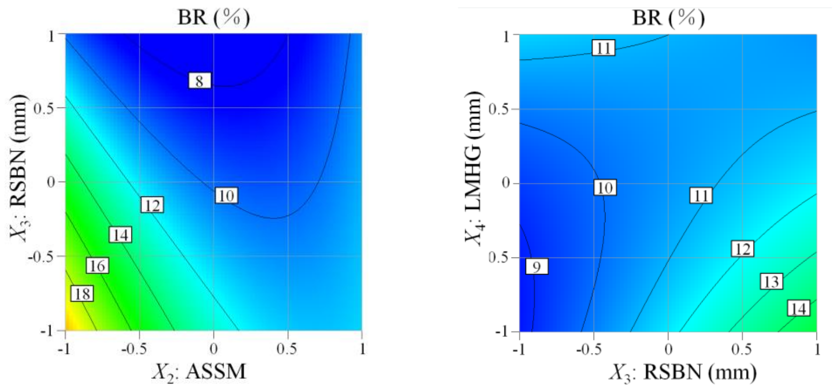


(a) $Y_2$=*f* (1, $X_2$, $X_3$, 1, 1) (b) $Y_2$=*f* (1, 1, $X_3$, $X_4$, 1)

**Figure 15.** Influence of interaction factors on test indicator $Y_2$.

To investigate the interactive factor $X_3X_4$, we fixed factor $X_3$, and set $X_1$ to 250 mm, $X_2$ as the rotary tillage knife, and $X_5$ as 200 mm. When $X_4$ is in the range 10–50 mm and $X_3$ is in the range 240–270 mm, the notch is small, resulting in poor passability of soil and straw. $Y_2$ increases with an increase in $X_4$ and is positively correlated. When $X_3$ is in the range 270–340 mm, $Y_2$ decreases with an increase in $X_4$ and is negatively correlated. A larger gap between the material hopper and the ground surface makes it easier for the soil broken by the opener to be discharged from the bottom of the side baffle, which reduces the BR.

**Discussion**

The limitations arising from the narrow spacing of rows for the no-tillage sowing of wheat mean that the sowing machine is more likely to experience blockage and shutdown than for corn. Moreover, it is challenging to apply existing anti-blocking and seed-belt-cleaning devices developed for corn to a wheat no-till planter by reducing the size of the device. In the Huang-Huai-Hai region of China, there is abundant rain during the winter sowing period for wheat. This means that the field straw and soil have a high water content, the crop straw is not easy to cut, the soil and straw are difficult to separate when wet, and the passability of the machine is poor. This situation has forced researchers to redesign the traditional concept of a no-till planter or to create an anti-blocking and cleaning function for the seeding belt of the machine by attaching additional intelligent electric control equipment, which is exceedingly timeconsuming and labor-intensive. In addition, farmers have difficulty adapting and applying this approach to actual production operations.

Our work shows that the passability and SRR of a no-till wheat planter can be significantly improved by installing an additional uncomplicated SSARD on an existing planter using innovative mechanical structure design methods. The results show that this approach can meet the agronomic requirements of no-tillage sowing of wheat in the Huang-Huai-Hai area of China.

Several limitations of the current research and more in-depth research directions for the future can be identified. There is a gap between the material hopper and the ground surface, and there is always a small proportion of the straw that can pass through this gap and fall onto the seeding belt, which makes it impossible to clean the straw from the seeding belt thoroughly. In future work, we will focus on the structural design of the straw baffle, the side baffle, and the material hopper. Further improvements could be made to the SRR of the seeding belt during operation by adding a secondary straw-cleaning mechanism or by designing a new straw hinder mechanism.

This paper has proposed a method of measuring the BR by discrete element simulation, and is the first to present a quantitative analysis method for the passability of a machine for no-tillage sowing. However, this study has not explored in detail the values of BR that lead to blocking and the corresponding relationship between the range of BR and the type of blockage. The next steps in our work plan include the establishment, analysis, and elaboration of a BR model.

**Determination of optimal parameters based on the regression model**

Since the ASSM consisted of three structural forms, the optimal solution for the model was obtained when $X_2$ was fixed at different values. In addition, optimization of the model involved solving for two indicators simultaneously, different weight grades were established for $Y_1$ and $Y_2$, and the importance of $Y_2$ was set higher than for $Y_1$ in the software. The optimization equations for the regression model were established as follows:

$$\begin{cases} \max Y_1 \\ \min Y_2 \\ 150 \le X_1 \le 250 \\ 240 \le X_3 \le 340 \\ 10 \le X_4 \le 50 \\ 100 \le X_5 \le 200 \end{cases} \tag{5}$$

Based on the theoretical analysis presented above and by solving Equation (5), the optimal parameter combinations were determined as follows: ODSB 250 mm, RSBN 340 mm, LMHG 10 mm, and WOSB 200 mm. When $X_2$ was fixed at −1 (i.e., no additional structure), the SRR was 100%, and the BR was 16.0%. When $X_2$ was set to zero (i.e., the additional notched disk knife), the SRR was 95.85%, and the BR was 12.23%. When $X_2$ = 1 (i.e., the additional rotary tillage knife), the SRR was 98.20%, and the BR was 14.78%.

**Field test verification**

**Passability of the machine**

Based on the three groups of results presented above, the SSARD with the corresponding parameter combinations was manufactured, and a field passability test was conducted. Figure 16 shows photographs of the field test site, and the results are shown in Table 6.

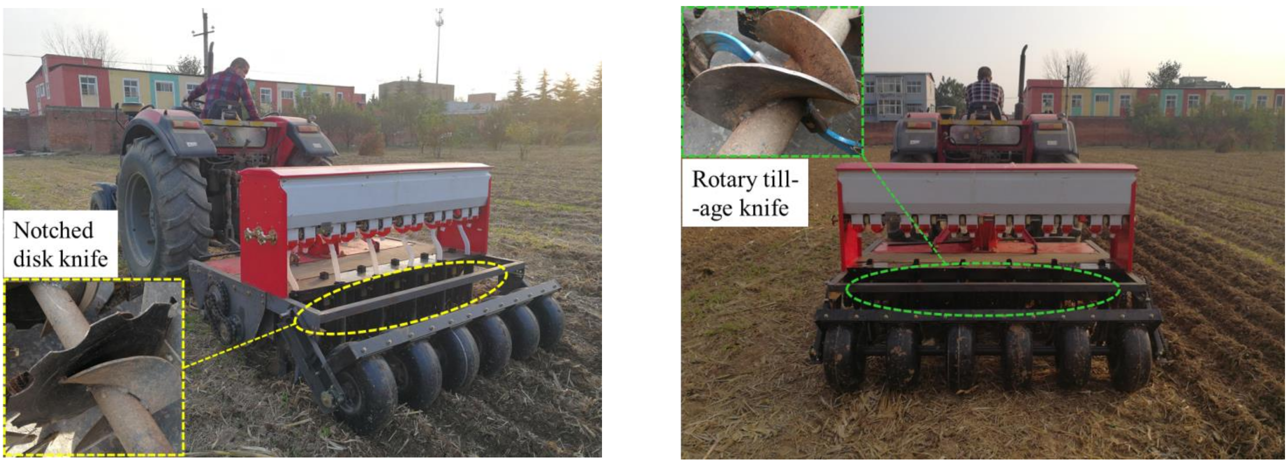


**Figure 16.** Photographs of the field verification test.

The test results showed that the field passability of the SSARD with ASSM was significantly improved. It was observed that the notched disk knife and the rotary tillage knife could form the effect of different rotary velocities, cutting and chopping the straw alternately with the no-till anti-blocking knife. This approach was able to clean the straw wrapped around the no-till anti-blocking knife. It could also break the clods accumulating on the inside of the straw baffle and the side baffle, in a timely manner. The passability of the machine and its operational stability were significantly improved, as shown in Movie 1.

**Table 6.** Field test results for the passability of the machine.

| Device type | No blockage /times | Slight blockage /times | General blockage /times | Severe blockage /times |
|---|---|---|---|---|
| No-till planter without SSARD | 0 | 1 | 1 | 1 |
| Optimized without additional structure | 1 | 2 | 0 | 0 |
| Optimized with additional notched disk knife | 3 | 0 | 0 | 0 |
| Optimized with additional rotary tillage knife | 3 | 0 | 0 | 0 |

### SRR for the seeding belt

The cleaning effect of the seeding belt is shown in Figure 17. Table 7 shows the actual test results for the SRR of the seeding belt.


(a) (b)

**Figure 17.** Straw cleaning effect of the seeding belt after the operation.

**Table 7.** Field test results for the straw cleaning effect of the seeding belt.

| Device type | Average SRR/% | Coefficient of variation |
|---|---|---|
| No-till planter without SSARD | 73.10 | 9.58 |
| Optimized without additional structure | 93.35 | 2.38 |
| Optimized with additional notched disk knife | 90.92 | 2.95 |
| Optimized with additional rotary tillage knife | 91.63 | 3.43 |

From Figure 17 and Table 7, it can be seen that the SRR of the optimized SSARD can reach 93.35%, a value 27.7% higher than the average SRR for the no-till planter without SSARD. After optimization, the SRR of the seeding belt of the machine was improved.

## Conclusions

This study explored the actual field operation performance of a contractualized spiral anti-blocking and grading device. First, in-depth research and theoretical analysis was conducted on its structure, to identify the key factors affecting the SRR and BR and their value ranges, which were determined as follows: ODSB ∈ [150,250] mm, ASSM ∈ [no additional structure; additional notched disk knife; additional rotary tillage knife], RSBN ∈ [240,340] mm, LMHG ∈ [10,50] mm, and WOSB ∈ [100,200] mm. Using the DEM, a quadratic rotational orthogonal combination simulation test was carried out, and a regression model for the effect of the test factors on evaluation indicators was established. The results indicated that the order of significance for the factors affecting SRR was ODSB＞LMHG＞RSBN＞WOSB＞ASSM, while for BR it was ASSM＞WOSB＞RSBN＞LMHG＞ODSB. Specifically, ASSM significantly reduced BR and improved the passability of the machine; increasing RSBN and WOSB reduced BR, with only a slight decrease in SRR; and decreasing LMHG increased SRR, with minimal negative impact on passability. Finally, the optimal operating parameter combination was determined as: ODSB = 250 mm, additional notched disk knife (for ASSM), RSBN = 340 mm, LMHG = 10 mm, and WOSB = 200 mm. Field verification tests showed that after optimization, the SSARD achieved an SRR of 93.35% (27.7% higher than for no-till planters without SSARD), with significantly improved passability. This optimal combination met the agronomic requirements for wheat no-tillage sowing in the Huang-Huai-Hai double cropping areas of China.

## Acknowledgements

The authors thank the Conservation Tillage Research Center for its support, and express sincere gratitude to Ms. Zhao Fuying, Mr. Li Peijun, and Ms. Wu Wenxia.

## Conflict of Interest

The authors declare that they have no known competing financial interests or personal relationships that could have appeared to influence the work reported in this paper.

## Data Availability Statement

The datasets generated and/or analyzed (including EDEM simulation data and field test data) are not publicly available, but support for accessing these datasets can be obtained by contacting the corresponding author.

## Funding

This work was supported by the National Natural Science Foundation of China (Grant No. 32401710), Study on wheat uniform-seeding mechanism for pneumatic pinhole tube seeding meter under wide-strip seedling zone system based on single-seed separating and stable feeding in low-position (CN) (Grant No.52175260), the China Agriculture Research System of MOF and MARA (CN) (Grant No.CARS-03), Innovative Research Team in University of China (CN) (Grant No.IRT13039), and the 2115 Talent Development Program of China Agricultural University and Chinese Universities Scientific Fund (CN) (Grant No.2021TC105).

## References

Baker, C. J., Saxton, K. E., Ritchie, W. R., Chamen, W. C. T., Reicosky, D. C., Ribeiro, M. F. S., Justice, S. E., & Hobbs, P. R. (2007). No-tillage seeding in conservation agriculture. *Experimental Agriculture*, *43*(4), 522–522. https://doi.org/10.1017/S0014479707005388

Gao, W. S. (2007). Development trends and basic principles of conservation tillage. *Scientia Agricultura Sinica*, *40*(12), 2702–2708. https://doi.org/10.3321/j.issn:0578-1752.2007.12.006

Hou, S., Zhu, Y., Zhu, X., Wang, Y., Ji, W., & Chen, H. (2022). Design and experiment of a straw clearing mulching no-tillage planter. *Biosystems Engineering*, *221*, 69–80. https://doi.org/10.1016/j.biosystemseng.2022.06.010

Fang, H., Ji, C., Tagar, A. A., Zhang, Q., & Guo, J. (2016a). Simulation analysis of straw movement in straw-soil-rotary blade system. *Transactions of the Chinese Society of Agricultural Machinery*, *47*(1), 60–67. https://doi.org/10.6041/j.issn.1000-1298.2016.01.009

Fang, H., Ji, C., Farman, A. C., Guo, J., Zhang, Q., & Chaudhry, A. (2016b). Analysis of soil dynamic behavior during rotary tillage based on distinct element method. *Transactions of the Chinese Society of Agricultural Machinery*, *47*(3), 7. https://doi.org/10.6041/j.issn.1000-1298.2016.03.004

Karayel, D., & Šarauskis, E. (2011). Effect of down force on the performance of no-till disc furrow openers for clay-loam and loamy soils. *Agricultural Engineering Research Papers*, *43*(3), 16–24.

Lampurlanés, J., Angás, P., & Cantero-Martínez, C. (2001). Root growth, soil water content and yield of barley under different tillage systems on two soils in semiarid conditions. *Field Crops Research*, *69*(1), 27–40. https://doi.org/10.1016/S0378-4290(00)00130-1

Li, H., Liu, H., Zhou, J., Wei, G., Shi, S., Zhang, X., Zhang, R., Zhu, H., & He, T. (2021). Development and first results of a no-till pneumatic seeder for maize precise sowing in Huang-Huai-Hai plain of China. *Agriculture*, *11*(10), 1023. https://doi.org/10.3390/agriculture11101023

Li, Y., Lu, C., Li, H., Wang, Z., Gao, Z., Wei, X., & He, D. (2022a). Design and experiment of symmetrical spiral row-sorting of the straw device based on kinematics analysis. *Agriculture*, *12*(7), 896. https://doi.org/10.3390/agriculture12070896

Li, Y., Lu, C., Li, H., He, J., Wang, Q., Huang, S., Gao, Z., Yuan, P., Wei, X., & Zhan, H. (2022b). Design and experiment of spiral discharge anti-blocking and row-sorting device of wheat no-till planter. *Agriculture*, *12*(4), 468. https://doi.org/10.3390/agriculture12040468

Liao, Q., Gao, H., & Shu, C. (2004). Present situations and prospects of anti-blocking technology of no-tillage planter. *Transactions of the Chinese Society of Agricultural Engineering*, *20*(1), 108–120. https://doi.org/10.3321/j.issn:1002-6819.2004.01.026

Lin, J., Li, B., & Li, H. (2015). Design and experiment of archimedes spiral type stubble breaking ditching device and stubble breaking anti blocking device. *Transactions of the Chinese Society of Agricultural Engineering*, *31*(17), 10–19. https://doi.org/10.11975/j.issn.1002-6819.2015.17.002

Liu, P., He, J., Li, Y., Li, H., Wang, Q., Lu, C., Zhang, Z., & Li, S. (2020). Design and experiment of double rollers maize stalk chopping device with different rotation speeds. *Transactions of the Chinese Society of Agricultural Engineering*, *36*(14), 69–79. https://doi.org/10.11975/j.issn.1002-6819.2020.14.009

Lu, C., Li, H., He, J., Zhu, H., & Xu, D. (2013a). Floated support anti-blocking device of wheat no-till seeder. *Transactions of the Chinese Society for Agricultural Machinery*, *44*(12), 52–153. https://doi.org/10.6041/j.issn.1000-1298.2013.12.009

Lu, C., He, J., Li, H., Wang, Q., Zhang, X., & Liu, J. (2013b). Finite element analysis and experiment on anti-blocking device based on support cutting. *Transactions of the Chinese Society for Agricultural Machinery*, *44*(1), 61–66. https://doi.org/10.6041/j.issn.1000-1298.2013.S1.012

McLaughlin, N. B., Campbell, A. J., & Owen, G. T. (2019). Performance of hoe and triple disc furrow openers on no-till grain drills in a fine sandy loam soil. *Soil and Tillage Research*, *195*, 104373. https://doi.org/10.1016/j.still.2019.104373

Niu, M., Fang, H., Chandio, F. A., Shi, S., Xue, Y., & Liu, H. (2019). Design and experiment of separating-guiding anti-blocking mechanism for no-tillage maize planter. *Transactions of the Chinese Society of Agricultural Machinery*, *50*(8). https://doi.org/10.6041/j.issn.1000-1298.2019.08.006

Ministry of Agriculture and Rural Affairs. (2009). NY/T 1768—2009《Technical specifications of quality evaluation for no-tillage drilling machinery. https://hbba.sacinfo.org.cn/stdDetail/e7eb27074b6ce08c92f8da0d70cd73559a869b61adafd485b32eb1546db6c745

Ministry of Agriculture and Rural Affairs. (2022). The Ministry of Agriculture and Rural Affairs issued the technical guidance for 2023 Northeast Black Land Conservation Farming Action Plan. http://www.gov.cn/xinwen/2022-10/29/content_5722481.htm

Ni, H. G., Lu, F. H., Luo, X. L., Tian, H. Y., Wang, J. Z., Guan, Y. F., Chen, S. J., Luo, X. J., & Zeng, E. Y. (2008). Assessment of sampling designs to measure riverine fluxes from the Pearl River Delta, China to the South China Sea. *Environmental Monitoring and Assessment*, *143*(1), 291–301. https://doi.org/10.1007/s10661-007-9982-x

Yuan, P., Li, H., Jiang, G., He, J., Lu, C., & Huang, S. (2021). Design and experiment of straw cleaning device for wide-narrow maize no-tillage sowing strip in drip irrigation area. *Transactions of the Chinese Society of Agricultural Machinery*, *52*(6), 43–52. https://doi.org/10.6041/j.issn.1000-1298.2021.06.005

Liu, P., He, J., Lou, S., Wang, Y., Zhang, Z., & Lin, H. (2021). Design and experiment for dynamic supporting type maize straw chopping retention device with different rotation speeds of disc blade. *Transactions of the Chinese Society of Agricultural Machinery*, *52*(10), 41–50. https://doi.org/10.6041/j.issn.1000-1298.2021.10.004

Wang, Q., Jia, H., Zhu, L., Li, M., & Zhao, J. (2019). Design and experiment of star-toothed concave disk row cleaners for no-till planter. *Transactions of the Chinese Society of Agricultural Machinery*, *50*(2), 68–77. https://doi.org/10.6041/j.issn.1000-1298.2019.02.008

Shi, Y., Rex, S. X., Wang, X., Hu, Z., Newman, D., & Ding, W. (2019). Numerical simulation and field tests of minimum-tillage planter with straw smashing and strip laying based on EDEM software. *Computers and Electronics in Agriculture*, *166*, 105021. https://doi.org/10.1016/j.compag.2019.105021

The State Council. (2020). The Ministry of Agriculture and Rural Affairs and the Ministry of Finance issued the Action Plan for Conservation Cultivation of Black Soil in Northeast China (2020-2025). http://www.gov.cn/xinwen/2020-03/18/content_5492780.htm

Uri, N., Atwood, J., & Sanabria, J. (1999). The environmental benefits and costs of conservation tillage. *Environmental Geology*, *38*, 111–125. https://doi.org/10.1007/s002540050407

Uri, N., Atwood, J., & Sanabria, J. (1998). An evaluation of the environmental costs and benefits of conservation tillage. *Environmental Impact Assessment Review*, *18*(6), 521–550. https://doi.org/10.1016/S0195-9255(98)00021-3

Wulantuya, Wang, C., Qi, S., Yan, J., & Wang, J. (2015). Test and analysis of performance of screw conveyor for rubbing and breaking corn straw. *Transactions of the Chinese Society of Agricultural Engineering*, *31*(21), 51–59. https://doi.org/10.11975/j.issn.1002-6819.2015.21.007

Wulantuya. (2016). Study on the mechanism of screw conveying theory for rubbing and breaking corn straw [Doctoral dissertation, Inner Mongolia Agricultural University].

Wang, X., Hu, H., Wang, Q., Li, H., He, J., & Chen, W. (2017). Calibration method of soil contact characteristic parameters based on DEM theory. *Transactions of the Chinese Society of Agricultural Machinery*, *48*(12), 78–85. https://doi.org/10.6041/j.issn.1000-1298.2017.12.009

Zhao, H., Li, H., Ma, S., He, J., Wang, Q., Lu, C., Zheng, Z., & Zhang, C. (2020). The effect of various edge-curve types of plain-straight blades for strip tillage seeding on torque and soil disturbance using DEM. *Soil and Tillage Research*, *202*, 104674. https://doi.org/10.1016/j.still.2020.104674

Zhao, S., Liu, H., Hou, L., Zhang, X., Yuan, Y., & Yang, Y. (2021). Development of deep fertilizing no-tillage segmented maize sowing opener using discrete element method. *Transactions of the Chinese Society of Agricultural Machinery*, *37*(13), 1–10. https://doi.org/10.11975/j.issn.1002-6819.2021.13.001